Indium induced band gap tailoring in Ag Ga 1 − x In x S 2 chalcopyrite structure for visible light photocatalysis

Jum Suk Jang, Pramod H. Borse, Jae Sung Lee, Sun Hee Choi, and Hyun Gyu Kim

Citation: The Journal of Chemical Physics **128**, 154717 (2008); doi: 10.1063/1.2900984

View online: http://dx.doi.org/10.1063/1.2900984

View Table of Contents: http://scitation.aip.org/content/aip/journal/jcp/128/15?ver=pdfcov

Published by the AIP Publishing

Indium induced band gap tailoring in $AgGa_{1-x}In_xS_2$ chalcopyrite structure for visible light photocatalysis

Jum Suk Jang,[1] Pramod H. Borse,[1] Jae Sung Lee,[1,a)] Sun Hee Choi,[2] and Hyun Gyu Kim[3]
[1]*Eco-friendly Catalysis and Energy Laboratory (NRL), Department of Chemical Engineering, Pohang University of Science and Technology, Pohang 790-784, Republic of Korea*
[2]*Beamline Research Division, Pohang Accelerator Laboratory, POSTECH, San 31, Hyojadong, Namgu, Pohang 790-784, Republic of Korea*
[3]*Busan Center, Korea Basic Science Institute (KBSI), Busan 609-735, Republic of Korea*

(Received 28 November 2007; accepted 27 February 2008; published online 21 April 2008)

Indium was substituted at gallium site in chalcopyrite $AgGaS_2$ structure by using a simple solid solution method. The spectroscopic analysis using extended x-ray absorption fine structure and x-ray photoelectron spectroscopy confirmed the indium substitution in $AgGaS_2$ lattice. The band gap energy of $AgGa_{1-x}In_xS_2$ ($x=0-1$) estimated from the onset of absorption edge was found to be reduced from 2.67 eV ($x=0$) to 1.9 eV ($x=1$) by indium substitution. The theoretical and experimental studies showed that the indium *s* orbitals in $AgGa_{1-x}In_xS_2$ tailored the band gap energy, thereby modified the photocatalytic activity of the $AgGa_{1-x}In_xS_2$. © *2008 American Institute of Physics*. [DOI: 10.1063/1.2900984]

I. INTRODUCTION

Visible light-driven photocatalysts have been actively investigated for the last few decades for hydrogen production via water splitting under solar radiation.[1–5] Especially, binary sulfides[6,7] are known for their efficient hydrogen production by water splitting due to their suitable band edge positions to reduce/oxidize water. In contrast, most of the oxide photocatalysts[8–11] possess the band structure that is not suitable for hydrogen production from water splitting. Nonetheless, there is not much work on water splitting by ternary sulfide photocatalysts. Recently, Tsuji *et al.* reported a systematic study of the photophysical properties (i.e., photocatalytic activities and band structure) of $(AgIn)_xZn_{2(1-x)}S_2$ systems.[12] We reported that $AgGaS_2$ and $AgGaS_2$/CdS nanobulk composite showed excellent activity for photocatalytic hydrogen production from electrolyte containing sulfide and sulfite under visible right irradiation ($\lambda \geqslant 420$ nm).[13,14]

In an effort to fabricate an efficient photocatalyst, we tried to modulate the band structure of $AgGaS_2$ by substitution of indium into the Ga site in the $AgGaS_2$ lattice. The $AgGaS_2$ is a *p*-type semiconductor with a direct band gap energy of ~2.68 eV. Indium substitution enhanced the visible light absorption of $AgGaS_2$ as desired for visible light photocatalysis. We synthesized $AgGa_{1-x}In_xS_2$ by a solid solution method under N_2 flow and further sintered the material under H_2S flow to remove any impurity phase.[13] We investigated the electronic structure of the $AgGa_{1-x}In_xS_2$ by computation of band structure and by experimental detection of the local structure around gallium by x-ray absorption fine structure (XAFS). These theoretical and experimental results were employed to explain the enhanced photoactivity of the ternary sulfide solid solutions.

a)Author to whom correspondence should be addressed. Electronic mail: jlee@postech.ac.kr.

II. EXPERIMENTAL SECTION

A. Synthesis of $AgGa_{1-x}In_xS_2$ photocatalyst

$AgGa_{1-x}In_xS_2$ ($x=0, 0.1, 0.25, 0.5, 0.75, 1.0$) samples were prepared by a conventional solid-state reaction based on our earlier reports.[13] Thus, stoichiometric amounts of Ag_2S (Aldrich 99.9%), Ga_2S_3 (10% excess, Aldrich 99.99%), and In_2S_3 (Aldrich 99.99%) were mixed and ground in a *mortar* in the presence of ethanol and dried in air. The pelletized powders were calcined at 1073 K for 5 h under N_2 flow and the resulting product was ground in a mortar in the presence of ethanol. The powders were further sintered to remove defects or impurity phases (if any) and to increase the crystallinity of the samples. An additional thermal treatment was carried out at 873–1123 K for 3 h under the 40 vol % H_2S/He flow (35 μmol/s).

B. Characterization

The crystalline phases of the final products were determined by x-ray diffraction (XRD) on a M18XHF diffractometer. The optical properties of photocatalyst powders were analyzed by UV-visible diffuse reflectance spectrometer (Shimadzu, UV 2401). The morphologies of the photocatalysts were investigated by field emission scanning electron microscopy (SEM) (Hitachi, S-4200) and transmission electron microscope (JEOL JEM 2010F, field emission electron microscope) instrument operated at 200 kV. The elemental analysis was carried out by using x-ray photoelectron spectroscopy (XPS) measurements (VG Scientific, ESCALAB 220iXL) using Mg $K\alpha$ radiation (1253.6 eV). The binding energy calibration was performed using Au 4*f* peak as the reference energy.

The local structure around Ga in $AgGa_{1-x}In_xS_2$ was characterized with x-ray absorption fine structure (XAFS). X-ray absorption measurements were conducted on the 7C1-

beamline of Pohang Accelerator Laboratory (PAL, 2.5 GeV, stored current of 120–180 mA). The radiation was monochromatized using a Si(111) double crystal monochromator and the incident beam was detuned by 15% using a piezoelectric translator to minimize the contamination from higher harmonics, in particular, the third order reflection of the silicon crystals. Since Ga metal foil was not available due to its low melting point, energy was calibrated with Ga_2O_3 first, and then all spectra were recalibrated later with respect to *K*-edge energy of Ga by using FEFF calculations.[14] The obtained data were analyzed using the IFEFFIT suite of software programs[15] and the FEFF 8.2 code.[14] The detailed procedure for data analysis is described elsewhere.[16–18]

The electronic band-structure calculation was performed by using the WIEN 97 package based on the full potential linearized augmented plane wave method.[19] This method uses the generalized gradient approximation, an improvement of the local spin-density approximation within density functional theory that is known to be an efficient and accurate scheme for solving the many-electron problem of a crystal. The crystallographic parameters for the calculation including lattice parameters and atomic positions were adopted from the literature.[20,21]

C. Photocatalytic hydrogen production

The photocatalytic reactions were carried out at room temperature under atmospheric pressure in a closed circulation system using a Hg-arc lamp (450 W) equipped with a UV cut-off filter ($\lambda \geqslant 420$ nm). The rate of H_2 evolution was determined in an aqueous solution (100 ml) containing 0.1 g catalyst and 0.1*M* $Na_2S+0.02M$ Na_2SO_3. The quantitative detection of H_2 evolution was done by gas chromatography (thermal conductivity detector, molecular sieve 5 Å column and Ar carrier). Before photocatalytic reaction, 1 wt % Pt was deposited on the photocatalysts by photodeposition method.[22]

III. RESULTS AND DISCUSSIONS

A. Solid solution between $AgGaS_2$ and $AgInS_2$

Figure 1 shows XRD patterns of $AgGa_{1-x}In_xS_2$ samples ($x=0-1.0$). Comparison of the patterns with standard JCPDS data shows that $AgGaS_2$ exhibits a tetragonal structure with lattice parameters of $a=5.7572$ and $c=10.3036$ Å.[20] The gradual shift of the main (112) peak toward lower diffraction angles with increasing indium content is correlated with the increment in the lattice constants to $a=5.8760$ and $c=11.2007$ Å, viz., the parameters of tetragonal $AgInS_2$ crystal structure according to the standard JCPDS. The small difference in the ionic radii of In^{3+} (0.80 Å) and Ga^{3+} (0.62 Å) ions suggests that there is a low probability of deformation of tetragonal unit cell, but the shift in the 2θ angle of diffraction is expected due to the lattice expansion. The gradual shift in the peak position indicates possible substitution of indium. Indeed, no other impurity phase was detected in the XRD pattern except for the last sample with the highest indium content, $AgInS_2$. The sample $AgGa_{1-x}In_xS_2$, ($x=1$) represents a mixture of orthorhombic and hexagonal phases, probably because it was prepared under the conditions optimized for the preparation of $AgGaS_2$. For the purpose of this work, it would have been better if a single phase $AgInS_2$ crystal structure were observed in the XRD pattern.

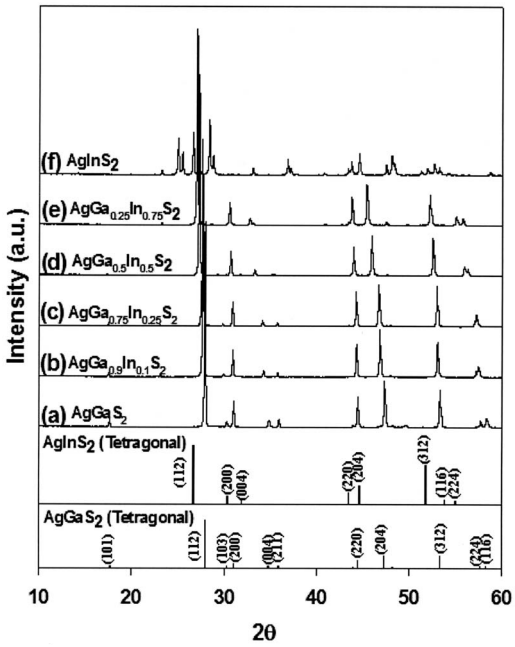

FIG. 1. X-ray diffraction patterns of $AgGa_{1-x}In_xS_2$ photocatalyst for $x=0$ (a), 0.1 (b), 0.25 (c), 0.5 (d), 0.75 (e), and 1.0 (f), along with the JCPDS data of $AgGaS_2$ and $AgInS_2$.

Figure 2(a) shows the UV-visible diffuse reflectance spectra of $AgGa_{1-x}In_xS_2$ samples ($x=0-1.0$). The redshift in the band edge with increase in x from 0 to 1.0 is clearly visible from the spectra, revealing that the band gap tuning has been realized by incorporation of indium in $AgGaS_2$ lattice. The band gap energies of $AgGa_{1-x}In_xS_2$ estimated from the absorption edges were found to decrease from 2.7 to 1.9 eV with increase in indium concentration in $AgGaS_2$ photocatalyst. The inset of the figure demonstrates that with increase in x value, the color of $AgGa_{1-x}In_xS_2$ changes from dark green, to yellow, orange, red, and finally to dark red. This is in accordance with the respective absorption spectra of Fig. 2(a). In addition to the concentration dependent band gap tuning in $AgGa_{1-x}In_xS_2$ samples ($x=0-1.0$), one cannot rule out a possible minor contribution to the absorption from the indirect optical transitions at very

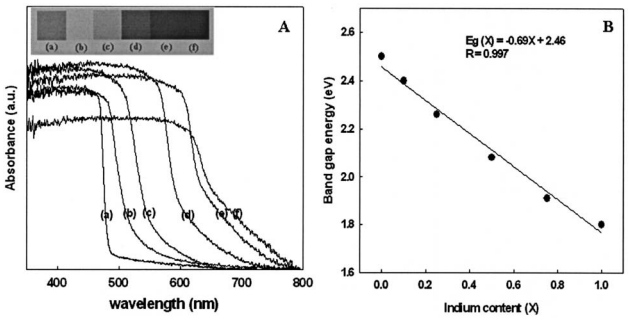

FIG. 2. (A) UV-visible, diffuse reflectance spectra of $AgGa_{1-x}In_xS_2$ photocatalyst for $x=0$ (a), 0.1 (b), 0.25 (c), 0.5 (d), 0.75 (e), and 1.0 (f). The inset shows colors of respective samples, (B) The graph of indium concentration in $AgGa_{1-x}In_xS_2$ versus the measured band gap energy.

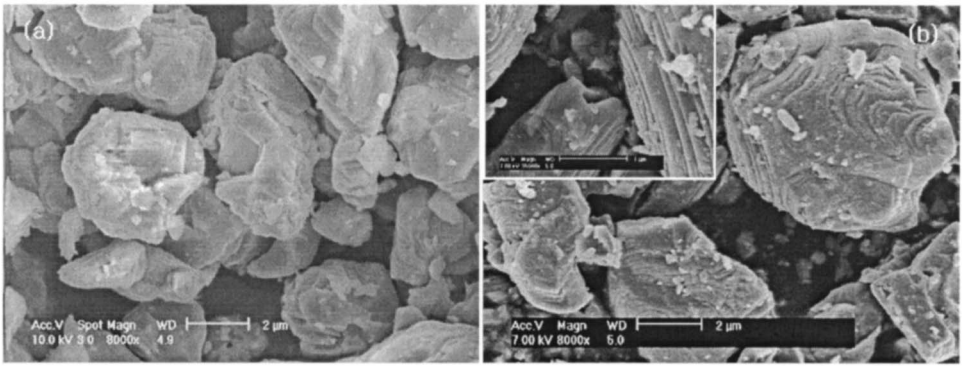

FIG. 3. The morphology of (a) $AgGaS_2$ and (b) $AgGa_{0.9}In_{0.1}S_2$ examined by SEM.

high dopant concentrations. Further, Fig. 2(b) clearly shows the quantitative correlation between the value of x (indium concentration) and the respective optical band gap energies estimated from the absorption edges, suggesting that there is a systematic redshift in the band gap energy with indium concentration. This redshift in the band edge enhances the visible light absorptivity of the photocatalyst. This, in turn, affects the photocatalytic activity of the material as described later.

Figure 3 shows morphological differences between $AgGaS_2$ and $AgGa_{0.9}In_{0.1}S_2$ particles. The $AgGaS_2$ sample shows irregular micron size particles (2–3 μm) with rough surfaces and edges. In contrast, the $AgGa_{0.9}In_{0.1}S_2$ sample shows particles made of well-defined steps. Such nanostructured edges were proposed to improve photocatalytic properties because the incident photon was not shielded and photogenerated electrons could easily migrate to the edge of the nanostructured step.[23] Thus, it appears that the enhanced photocatalytic activity of $AgGa_{0.9}In_{0.1}S_2$ upon indium substitution originates not only from the increased optical absorption but also as a consequence of indium-favored nanostep formation.

XPS measurements were carried out to analyze the oxidation state of Ga and In atoms in $AgGa_{1-x}In_xS_2$ photocatalysts. Figure 4 shows the core level spectra of Ga $2p$ and In $3d$ for $AgGa_{1-x}In_xS_2$ (x=0–0.75). Figure 4(a) indicates the doublet splitting of Ga $2p$ orbital into $2p_{3/2}$ and $2p_{1/2}$ bands revealing the trivalent oxidation state of Ga. Further, with the reduction in Ga concentration in $AgGa_{1-x}In_xS_2$, the intensity of these peaks decreased. On the contrary, the intensity of In $3d_{5/2}$ and $3d_{3/2}$ peaks was found to increase in Fig. 4(b). The respective binding energies are attributed to the existence of trivalent gallium and indium in $AgGa_{1-x}In_xS_2$. The attribution was validated with further spectroscopic studies using x-ray absorption near-edge spectroscopy (XANES) as described below.

XAFS experiments were performed in order to investigate changes in the local structure around Ga in $AgGa_{1-x}In_xS_2$. Figure 5 shows Ga K-edge XANES of $AgGa_{1-x}In_xS_2$ (x=0,0.1,0.25,0.5). The rising feature of the Ga K-edge absorption denoting the electronic transition from $1s$ to $4p$ orbitals remained invariant in its position despite of increasing the amount of indium. Since the absorption edge energy is indicative of the formal oxidation state of an absorbing element, there is no change of the formal state of Ga^{3+}, although some Ga^{3+} is replaced with In^{3+} in $AgGa_{1-x}In_xS_2$. However, the absorption peak a shows slightly reduced intensities with increasing x in $AgGa_{1-x}In_xS_2$. The second oscillation peak b above the Ga K-edge absorption shifts to a lower energy as more indium atoms are introduced to $AgGa_{1-x}In_xS_2$.

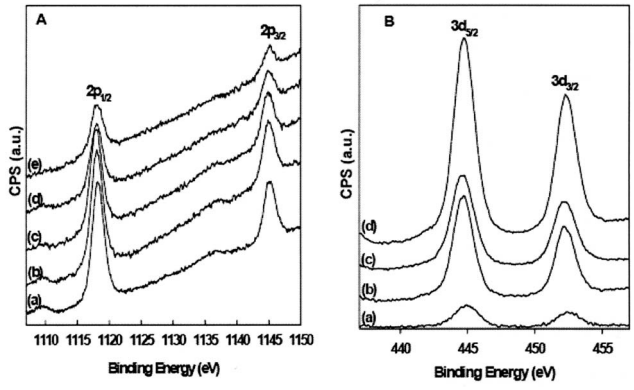

FIG. 4. The XPS core-level spectra of (A) Ga $2p$, (B) In $3d$ in $AgGa_{1-x}In_xS_2$ samples. The respective value of x for (A) Ga as (a) 0.0, (b) 0.1, (c) 0.25, (d) 0.5, and (e) 0.75 and (B) In as (a) 0.1, (b) 0.25, (c) 0.5, and (d) 0.75.

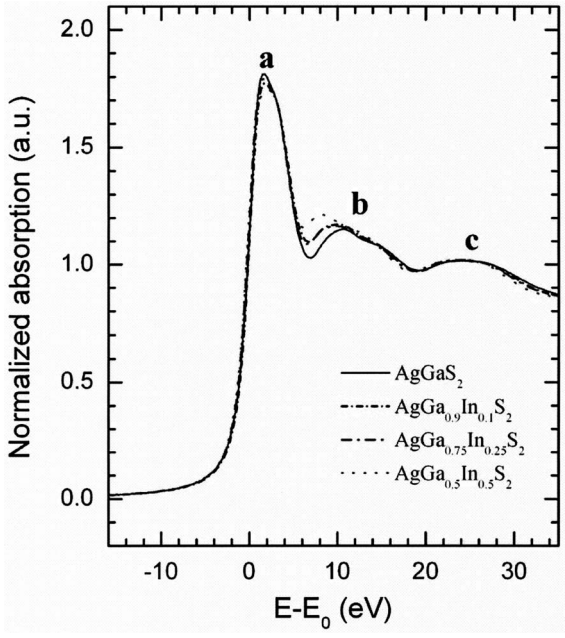

FIG. 5. Ga K-edge XANES spectra of respective $AgGa_{1-x}In_xS_2$ samples for $x\sim$0, 0.1, 0.25, and 0.5.

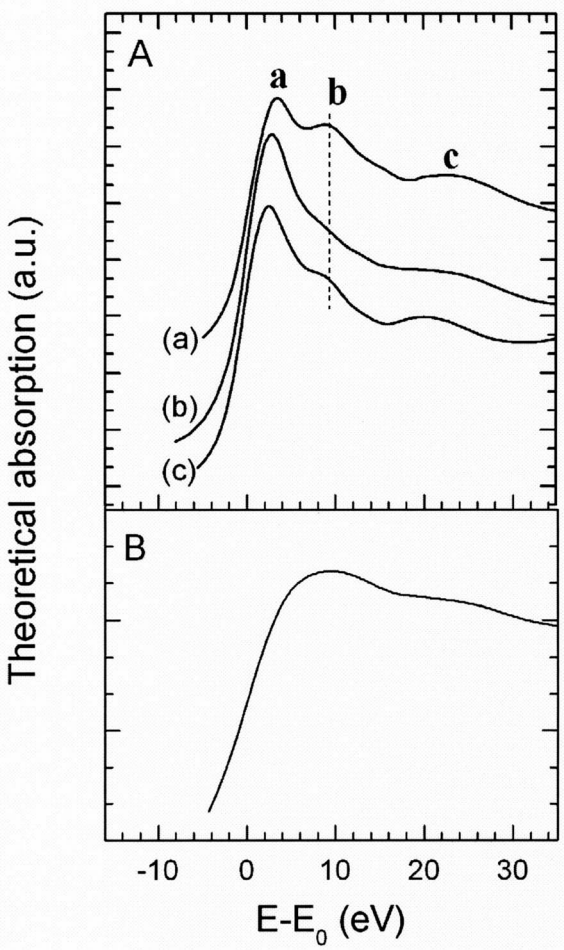

FIG. 6. (A) Theoretically calculated Ga *K*-edge XANES spectra of (a) $AgGaS_2$ in its own lattice, (b) $AgGaS_2$ without the second shell of Ga—M (M=Ag, Ga, or In), and (c) $AgGaS_2$ in $AgInS_2$ lattice. (B) Theoretically calculated In *K*-edge XANES spectrum of $AgInS_2$.

To interpret the observed features, we calculated theoretical spectra by using FEFF 8 code for three possible structures. Both $AgGaS_2$ and $AgInS_2$ are the I-III-VI family with the chalcopyrite structure.[20,24] A difference between the compounds is the larger lattice constants for $AgInS_2$ by 0.1188 and 0.8971 A in the *a* and *c* axes, respectively. Therefore, we compared the Ga *K*-edge XANES of $AgGaS_2$ in its own lattice with that of $AgGaS_2$ in the $AgInS_2$ lattice. The FEFF calculations were performed by using the Hedin-Lundqvist self-energy with 1 eV experimental broadening. A radius of 4.2 A was chosen for the self-consistent potential, ensuring that Ag and Ga atoms or Ag and In atoms of the second shell were all considered in the calculation of the spectrum. Full multiple scattering of a single electron was calculated for a cluster of 75 atoms for $AgGaS_2$ in its own lattice and of 71 atoms for the one in the $AgInS_2$ lattice.

Figure 6 shows the theoretical Ga *K*-edge XANES spectra for $AgGaS_2$ in its own lattice (a) and for the hypothetical $AgGaS_2$ in which the bond distances are elongated as much as those in $AgInS_2$ (c). While the oscillation peak *c* does not change, peak *b* moves to a lower energy of 16.8 from 19.7 eV with increasing bond length in $AgGaS_2$. To identify the origin of the oscillation peak *b*, we also calculated the theoretical XANES spectrum of $AgGaS_2$ with eliminating the scatterings from the surrounding metal atoms of Ag and Ga at 3.86–4.07 A. Different from (a) and (c) spectra, there is no peak *b* in the calculated spectrum. The XANES feature of the metal-metal coordination associated with the oscillation peak-*b* has been mentioned in the studies for R_2O_3 (R =rare-earth metal) and high T_c superconductor such as $RBa_2Cu_3O_{7-x}$.[25,26] Since the continuum resonance peak moves to a higher energy with decreasing bond length, the shift of peak *b* in Fig. 5 reveals that the substitution of some indium atoms induces the increased bond distances between Ga and directly coordinated metal backscatters. The second shell in $AgGaS_2$ comprises of three types of scatterings, i.e., (i) four Ga–Ag pairs at 3.86 A, (ii) four Ga–Ga pairs at 3.86 A, and (iii) four Ga–Ag pairs at 4.07 A. Considering that In substitution takes place at Ga^{3+} site, the shift of peak *b* could be attributed to the increased bond length of Ga–Ga or Ga–In. The slight decrease in the absorption peak *a* in Fig. 5 may be caused by the difference in electronic configurations of Ga^{3+} and In^{3+}. While the outermost occupied orbital is 3*d* for Ga^{3+}, it is 4*d* orbital for In^{3+}. The absorption feature of In *K*-edge for $AgInS_2$ is also simulated as shown in Fig. 6. The theoretical spectrum of $AgInS_2$ agrees with the one reported in the literature.[27] It is well known that 4*d* transition metals have much lower intensity at the absorption edge than 3*d* metal atoms.

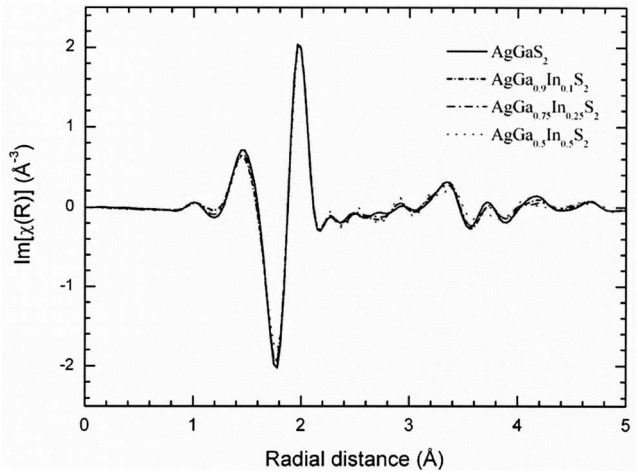

FIG. 7. Imaginary functions of Fourier-transformed $k^3\chi(k)$ for respective $AgGa_{1-x}In_xS_2$ samples with $x=0$, 0.1, 0.25, and 0.5.

The Fourier-transformed extended x-ray absorption fine structure (EXAFS) spectra of $AgGa_{1-x}In_xS_2$ in Fig. 7 confirm conclusions derived from XANES results. Imaginary functions in Fourier transforms of $k^2\chi(k)$ reflects the backscattering element contributing to a given shell and it is more sensitive to the local structure around Ga atoms than magnitude functions. The imaginary functions are almost identical up to 5 A except a minor difference in their intensity, regardless of the amount of introduced indium. The increased bond length of Ga–Ga or Ga–In revealed in the XANES is hardly observed in the Fourier-transformed EXAFS spectra because the twelve pairs of Ga–M (M=Ag, Ga, or In) scatterings constitute the second shell of $AgGa_{1-x}In_xS_2$ and thus, a small change in the interatomic distance for a specific bond tends to be covered up.

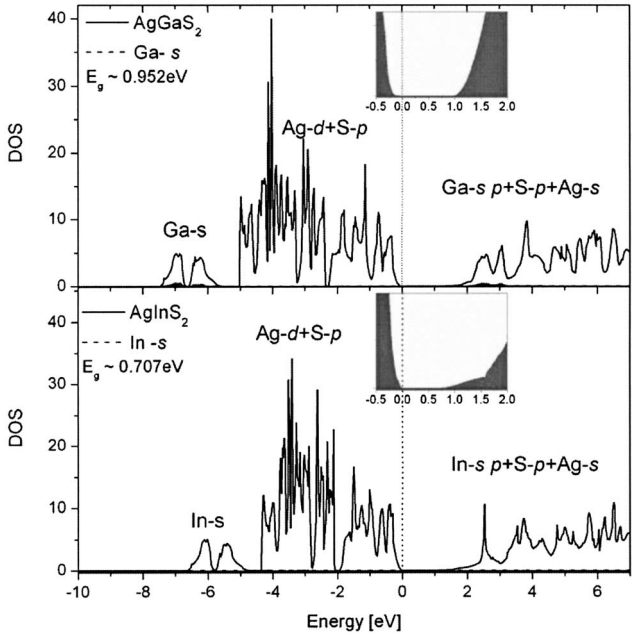

FIG. 8. Theoretically calculated total density of states (DOS) for $AgGaS_2$ and $AgInS_2$. The top of the valence band was set to 0 eV. The inset shows the finer details near respective band gaps.

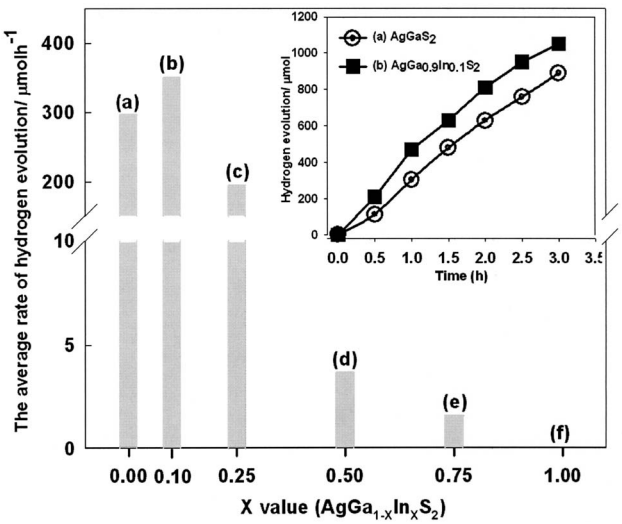

FIG. 9. The average rate of H_2 evolution over $AgGa_{1-x}In_xS_2$ [x=0 (a), 0.1 (b), 0.25 (c), 0.5 (d), 0.75 (e), and 1.0 (f)] from an electrolyte solution containing 0.1M Na_2S and 0.02M Na_2SO_3 under visible light irradiation. Catalysts: 0.1 g loaded 1 wt % Pt, Light source: Hg-arc lamp (500 W), equipped with IR liquid filter and with UV cut-off filter ($\lambda \geqslant 420$ nm). The inset shows the time course of H_2 production on 1 wt % Pt-loaded $AgGa_{1-x}In_xS_2$ samples [x=0.0 (a) and 0.1 (b)] under visible light illumination. Catalysts: 0.1 g loaded 1 wt % Pt; electrolyte: 0.1M Na_2S+0.02M Na_2SO_3, Light source: Hg-arc lamp (500 W) equipped with IR liquid filter and with UV cut-off filter ($\lambda \geqslant 420$ nm).

B. Computed electronic band structure

Figure 8 shows the total densities of states (DOS) for $AgGaS_2$ and $AgInS_2$, where the top of the valence band was set to 0 eV. The insets show the expanded regions near the band gap to clearly display the contribution of Ga/In partial DOS in modification of the band gap. The muffin-tin radii for Ag, Ga/In, and S were chosen to be 2.2, 2.0, and 1.8, respectively, in these calculations. The convergence parameter of RK_{max} was set to 8.0. The calculation was iterated with the charge convergence criteria of 0.0001. The atomic coordinates for WIEN97 calculation were adopted from literature.[20,21] The qualitative comparison of the DOS of two respective systems implies that valence band is a mixture of S 3p and Ag d orbitals. The top of valence band has a dominant contribution from S 3p. The respective conduction band is comprised of Ga/In s, S p, and Ag s orbitals, the bottom of conduction band being mainly made of Ga/In s orbital. The main difference in the DOS is the effect of In s contribution in narrowing the band gap of $AgInS_2$ compared to $AgGaS_2$. Effectively, we can conclude that the replacement of Ga with indium into the $AgGaS_2$ structure displaces the bottom of conduction band toward the lower energy.

C. Photocatalytic performance of $AgGa_{1-x}In_xS_2$ ($x \sim 0-1$)

Figure 9 shows the rate of H_2 evolution from $AgGa_{1-x}In_xS_2$ ($x \sim 0-1$) in the presence of an electrolyte (0.1M Na_2S and 0.02M Na_2SO_3) under visible light irradiation ($\lambda \geqslant 420$ nm). The photocatalytic activities of $AgGa_{1-x}In_xS_2$ samples were dependent on their compositions with the maximum activity for $AgGa_{0.9}In_{0.1}S_2$. Thus, with the increase in the value of x, the average rate of H_2 production reached the maximum of 350 μmol/h for $x \sim 0.1$ and then declined to 3.67 μmol/h for x=0.5 and finally to no hydrogen production for x=1.0. This indicates that there is an optimum concentration of indium required to be substituted at gallium site, which leads to the maximum yield of H_2 under visible light ($\lambda \geqslant 420$ nm) irradiation from water containing sulfide and sulfite ions as hole scavengers. The inset in Fig. 9 shows the time course of H_2 production over 1 wt % Pt-loaded $AgGa_{1-x}In_xS_2$ samples (x=0 and 0.1) under visible light illumination. The cocatalyst Pt loaded on semiconductor photocatalysts is known to enhance the rate of the hydrogen production. The Pt island over photocatalyst surface yields effective electron traps due to formation of a Schottky barrier at metal/semiconductor interface. This, in turn, is responsible for the efficient separation of photogenerated electrons and holes and thus an enhanced hydrogen production rate. Accordingly, the average rates were found to be 295 and 350 μmol/h at x=0.0 and 0.1, respectively. Photocatalytic hydrogen production increased steadily with increasing photoreaction time on both $AgGaS_2$ and $AgGa_{0.9}In_{0.1}S_2$. Therefore, it can be considered that they are stable for photocatalytic reaction in the presence of sulfite and sulfide solution under visible light irradiation.

The dependence of the rate of H_2 production on the indium concentration could be due to the change in the band structure, and hence utilization of the longer wavelengths. The band gap tailoring by indium substitution in $AgGa_{0.1}In_{0.9}S_2$ leads to a reduced band gap and thus higher photon absorption compared to that of the original material under the same illumination. Yet, the activity for H_2 production decreased when x is larger than 0.1 because the position of the conduction band of $AgGa_{1-x}In_xS_2$ (x=0.25–1.0) shifted toward more positive region as schematically shown

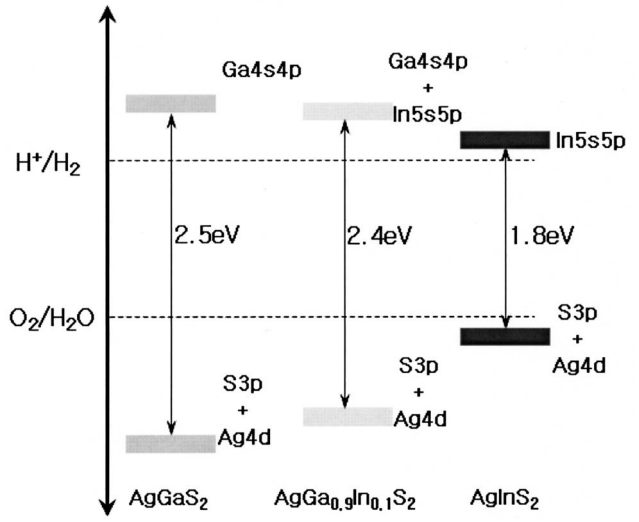

FIG. 10. Proposed schematic band structures for $AgGaS_2$, $AgGa_{0.9}In_{0.1}S_2$, and $AgInS_2$.

in Fig. 10. In addition, more diffuse DOS population near the bottom of conduction band of $AgInS_2$ may have hindered the hydrogen evolution for $AgGa_{1-x}In_xS_2$.

In Fig. 10, we propose the schematic of band structure for $AgGaS_2$, $AgG_{0.9}In_{0.1}S$, and $AgInS_2$ from the spectroscopic and the simulated electronic structure studies. The substitution of indium in the $AgGaS_2$ crystal lattice modifies the band energetics of $AgGa_{1-x}In_xS_2$ due to the contribution of In *s p* orbitals in the formation of the bottom of the conduction band. This seems to render a favorable shift of conduction bands in the $AgGa_{1-x}In_xS_2$ which is necessary for the hydrogen production using wider spectrum of visible light. However, indium substitution also shifts the conduction band to a more positive region decreasing the potential difference from water reduction. Thus, excessive indium substitution would hamper the photocatalytic activity as observed. Eventually, $AgInS_2$ is totally inactive although it has most favorable bandgap energy for visible light absorption. Thus, in addition to the band gap energy, this result emphasizes the importance of band positions relative to water reduction potentials for optimized photocatalysis for hydrogen production from water.

IV. CONCLUSION

Indium was substituted into Ga site in $AgGaS_2$ crystal lattice yielding an impurity-free solid solution phase by using a solid-state reaction method. The spectroscopic analysis using EXAFS and XPS confirmed the indium substitution in $AgGaS_2$ lattice. The concentration dependent band gap tuning was achieved in $AgGa_{1-x}In_xS_2$ $(x\sim 0-1)$, which was found to vary from 2.6 to 1.9 eV due to the participation of In $5s5p$ orbitals in the formation of the bottom of conduction band. The photocatalytic activity for hydrogen production over $AgGa_{1-x}In_xS_2$ showed the maximum value for $AgGa_{0.9}In_{0.1}S_2$.

ACKNOWLEDGMENTS

This work was supported by the Hydrogen Energy R&D Center, one of the 21st Century Frontier R&D Program, General Motors R&D Center, and BK-21 program.

[1] H. G. Kim, P. H. Borse, W. Choi, and J. S. Lee, Angew. Chem., Int. Ed. **44**, 4585 (2005).
[2] H. G. Kim, D. W. Hwang, and J. S. Lee, J. Am. Chem. Soc. **29**, 126 (2004).
[3] K. Maeda, K. Teramura, D. Lu, T. Takata, N. Saito, Y. Inoue, and K. Domen, Nature (London) **440**, 295 (2006).
[4] K. Maeda, K. Teramura, D. Lu, N. Saito, Y. Inoue, and K. Domen, Angew. Chem., Int. Ed. **45**, 7806 (2006).
[5] J. S. Jang, H. G. Kim, V. R. Reddy, S. W. Bae, S. M. Ji, and J. S. Lee, J. Catal. **231**, 213 (2005).
[6] N. Buhler, K. Meier, and J. F. Reber, J. Phys. Chem. **88**, 3261 (1984).
[7] S. A. Naman and M. Grätzel, J. Photochem. Photobiol., A **77**, 249 (1994).
[8] H. Kato, K. Asakura, and A. Kudo, J. Am. Chem. Soc. **125**, 3082 (2003).
[9] H. G. Kim, D. W. Hwang, J. Kim, Y. G. Kim, and J. S. Lee, Chem. Commun. (Cambridge) **1999**, 1077.
[10] P. H. Borse, U. A. Joshi, S. M. Ji, J. S. Jang, J. S. Lee, E. D. Jeong, and H. G. Kim, Appl. Phys. Lett. **90**, 034103 (2007).
[11] P. H. Borse, J. S. Lee, and H. G. Kim, J. Appl. Phys. **100**, 124915 (2006).
[12] I. Tsuji, H. Kato, and A. Kudo, Angew. Chem., Int. Ed. **44**, 3565 (2005).
[13] I. Tsuji, H. Kato, H. Kobayashi, and A. Kudo, J. Phys. Chem. B **109**, 7323 (2005).
[14] A. L. Ankudinov, C. Bouldin, J. J. Rehr, J. Sims, and H. Hung, Phys. Rev. B **65**, 104107 (2002).
[15] M. Newville, J. Synchrotron Radiat. **8**, 322 (2001).
[16] E. D. Park, S. H. Choi, and J. S. Lee, J. Phys. Chem. B **104**, 5586 (2000).
[17] S. H. Choi, B. R. Wood, J. A. Ryder, and A. R. Bell, J. Phys. Chem. B **107**, 11843 (2003).
[18] D. E. Sayer and B. A. Bunker, in *X-ray absorption: Principles, Applications, Techniques of EXAFS, SEXAFS and XANES*, edited by D. C. Koningsberger and R. Prins (Wiley, New York, 1988), p. 211.
[19] P. Blaha, K. Schwarz, and J. Luitz, WIEN97, A Full Potential Linearized Augmented Plane Wave Package for Calculating Crystal Properties, Techn. Universität Wien, Wien, Austria, 1999.
[20] S. C. Abrahams and J. L. Bernstein, J. Chem. Phys. **59**, 1625 (1973).
[21] J. L. Shay and J. H. Wernick, *Ternary Chalcopyrite Semiconductor: Growth, Electronic Properties and Applications* (Pergamon, Oxford, 1974).
[22] J. F. Reber and M. Rusek, J. Phys. Chem. **90**, 824 (1986).
[23] I. Tsuji, H. Kato, H. Kobayashi, and A. Kudo, J. Am. Chem. Soc. **126**, 13406 (2004).
[24] G. Delgado, A. J. Mora, C. Pineda, and T. Tinoco, Mater. Res. Bull. **36**, 2507 (2001).
[25] Y. Jeon, F. Lu, H. Jhans, S. A. Shaheen, and M. Croft, J. Appl. Phys. **63**, 4190 (1988).
[26] Y. Jeon, F. Lu, H. Jhans, S. A. Shaheen, G. Liang, M. Croft, P. H. Ansari, K. V. Ramanujachary, E. A. Hayri, S. M. Fine, S. Li, X. H. Feng, M. Greenblatt, L. H. Greene, and J. M. Tarascon, Phys. Rev. B **36**, 3891 (1987).
[27] F. Haass, M. Bron, H. Fuess, and P. Claus, Appl. Catal., A **318**, 9 (2007).